Appl. Phys. B 91, 349–352 (2008)
DOI: 10.1007/s00340-008-3012-8

Applied Physics B
Lasers and Optics

B. KIBLER[1,2]
R. FISCHER[3]
G. GENTY[4]
D.N. NESHEV[3]
J.M. DUDLEY[1,✉]

Simultaneous fs pulse spectral broadening and third harmonic generation in highly nonlinear fibre: experiments and simulations

[1] Département d'Optique P.M. Duffieux, Institut FEMTO-ST, CNRS-Université de Franche-Comté, UMR 6174, Besançon, France
[2] Département Optique, Interaction Matière Rayonnement, Institut CARNOT de Bourgogne, CNRS-Université de Bourgogne UMR 5209, 21078 Dijon, France
[3] Nonlinear Physics Centre, Research School of Physical Sciences and Engineering, Australian National University, 0200 ACT Canberra, Australia
[4] Tampere University of Technology, Institute of Physics, Optics Laboratory, 33101 Tampere, Finland

Received: 4 December 2007
Published online: 16 April 2008 •

ABSTRACT Experiments and numerical simulations are used to study non-phasematched single-mode third harmonic generation occurring simultaneously with fs pulse spectral broadening in highly nonlinear fibre. Pump pulses around 100 fs at 1560 nm injected into sub-5 cm lengths of commercially-available highly nonlinear fibre are observed to undergo spectral broadening spanning over 700 nm at the −30 dB level, and to simultaneously generate third harmonic radiation around 520 nm. Simulations based on a generalized nonlinear envelope equation are shown to well reproduce the spectral structure of the broadened pump pulses and the generated third harmonic signal.

PACS 42.65.-k; 42.81.Dp

1 Introduction

The physics of nonlinear propagation effects in novel optical waveguides and photonic structures is a subject that continues to attract intense interest [1–4]. Much of this recent work has been motivated by experiments in highly nonlinear and photonic crystal fibres, where the combination of engineered dispersion and elevated nonlinearity has led to the generation of broadband supercontinuum spectra that have found many important applications [5–9]. The spectral broadening associated with supercontinuum generation is now well-understood, and develops from the combination of nonlinear effects such as soliton fission, stimulated Raman scattering and four wave mixing [10]. In addition to these processes arising from the intensity-dependent Kerr nonlinearity, there has been growing interest in the dynamics of third harmonic generation (THG) that depends on the full field-dependent $\chi^{(3)}$ material response. Although studies have mostly focussed on THG generated under multimode phase-matching conditions [11–24], recent theoretical work has also incorporated harmonic generation into generalized nonlinear envelope equation simulations of ultrashort pulse propagation under single mode non-phasematched conditions [25]. This modelling approach is particularly relevant in extending envelope-based models of pulse propagation into a regime free of bandwidth constraints, but has not yet been the subject of any comparison with experimental work.

Our objective in this paper is to present just such a comparison between experimental investigations and generalized nonlinear envelope equation simulations for the particular case where sub-100 fs pulse propagation in highly nonlinear fibre (HNLF) results in significant spectral broadening, and the simultaneous generation of non-phasematched third harmonic radiation. Specifically, we report a comparison of the output spectral characteristics over the range 500–1670 nm for a fibre length of 600 μm where only one distinct THG peak is observed, as well as for a longer fibre length of 4.5 cm where two peaks around the THG wavelength appear in the spectrum. In both cases, the measured spectral structure is well-reproduced by the numerical simulations, confirming the validity of the generalized envelope equation approach to modelling spectral broadening to the third harmonic wavelength range.

2 Experiments

Our experiments used a passively-modelocked oscillator/amplifier fibre laser system (Precision Photonics PPL) producing pulses at 1560 nm with a 35 MHz repetition rate. The output pulses after propagation through a 1 m long SMF-28 fibre pigtail were characterized using second harmonic generation frequency resolved optical gating (FROG) and the pulse duration (FWHM) was found to vary over the range 90–110 fs as the (amplified) average output power was varied over the range 30–60 mW. The pulses at the end of the SMF-28 fibre were close to transform-limited with a −3 dB spectral width (FWHM) of around 70 nm but a small low-amplitude spectral pedestal on the pulses could be observed at intensities of −50 dB relative to the pump. A short length of speciality HNLF (OFS Denmark) was spliced to the SMF-28

✉ Fax: +33-3-81-66-64 23, E-mail: john.dudley@univ-fcomte.fr

pigtail and it was in this HNLF segment that both spectral broadening of the pump pulse and THG was observed. More parameters of this fibre are given below. The splice loss between the SMF-28 and HNLF was typically less than 0.2 dB, and we carefully checked that no THG signal was present at the output of the SMF-28 pigtail in the absence of the HNLF segment.

A similar setup was also used in our previous experiments that were carried out in the context of pulse compression using longer HNLF fibre segments of length 4–10 cm [26]. These experiments excited higher order solitons in the HNLF at average pump powers in the range 30–60 mW. It was also noticed that the spectral broadening of the pump pulses in the HNLF was accompanied by the generation of a THG signal but, although this could be clearly observed visually, no quantitative characterization was performed. In the present experiments, the spectrum of both the 1560 nm pump pulses and the generated signal around the third harmonic of 520 nm were measured simultaneously using a broadband optical spectrum analyser (Anritsu MS9702B) with 5 nm spectral resolution over the range 500–1670 nm. In addition, the spatial characteristics of the THG signal were measured by imaging the fibre endface with a CCD camera. From the spatial characterisation it was confirmed that the THG was generated in the fibre fundamental mode. The maximum average power of the output THG component at 520 nm was also measured to be ~ 50 nW.

Figure 1 shows typical results obtained for 50 mW average pump power and a 4.5 cm HNLF segment, showing both the broadened pump spectrum as well as the generated THG component. Although the optical spectrum analyser sensitivity limits restrict our measurements of the broadened pulse spectrum to wavelengths beyond 1670 nm, we note nonetheless that the pump broadening (due to soliton dynamics) extends over more than 700 nm at the -30 dB level. Around the third harmonic wavelength, we note a distinct component at 520 nm (the exact third harmonic of the central pump wavelength) as well as a second frequency-shifted peak at 575 nm that arises from the combined effects of pump spectral broadening and pump-THG group velocity mismatch [19, 20].

Our observations that the THG signal was generated in the fibre fundamental mode suggested a non-phasematched generation process and this was confirmed through additional measurements of modal and power characteristics as the spliced HNLF segment was cut back progressively to a minimum length of 600 μm. Note that this was carried out using standard cleaving techniques under a microscope. Figure 2a shows the measured spectrum at the output of the 600 μm HNLF segment, with the inset showing the imaged near field mode profile at the THG wavelength. The sharp peak at 980 nm is residual cw radiation from the erbium fibre amplifier pump, and the broad low amplitude pump spectral pedestal on the pulses from the oscillator/amplifier source can also be seen.

Note at this shorter segment length, only one distinct peak at the expected third harmonic wavelength was observed in the spectrum. The dependence on input pulse peak power was then measured by increasing input pulse power from 38 to 58 mW in 5 mW steps, and the increase in the generated THG component at 520 nm was measured

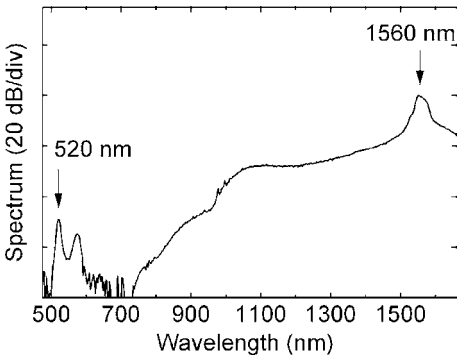

FIGURE 1 Experimental spectrum showing both the broadened pump spectrum and generated THG signal. The observed splitting of the generated THG signal is discussed in the text

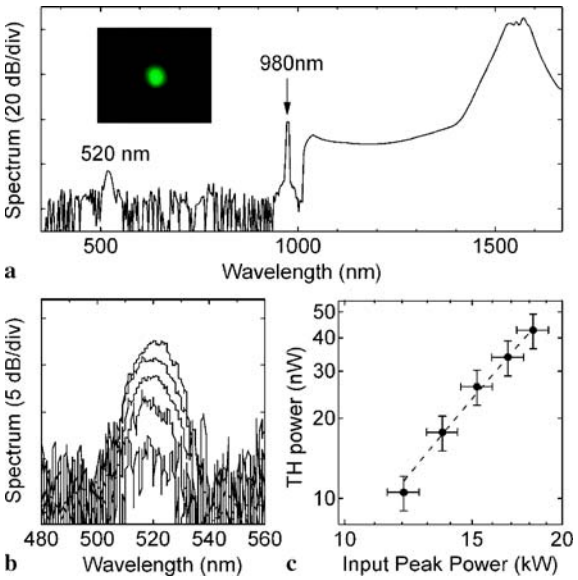

FIGURE 2 (**a**) Experimental spectrum measured at the output of 600 μm of HNLF for 50 mW input power. The *inset* shows the (green) observed mode profile of THG components. (**b**) Experimental spectra of THG components centred at 520 nm obtained by increasing input pulse power from 38 to 58 mW in 5 mW steps. (**c**) Experimental third harmonic signal power as a function of input pump power (with error bars) compared with a cubic fit (*dashed line*). Numerical simulations modelling the generation of THG power as a function of input pulse power for this case yield results that are indistinguishable from this fitted *dashed line*

on the spectrum analyser as shown in Fig. 2b. The quantitative dependence of the THG power on the corresponding input pulse peak power is shown in Fig. 2c using a log–log representation to plot the experimental results that are shown with error bars. The dashed line is obtained from numerical simulations as described below and follows the cubic dependence expected from a third-order nonlinear process.

3 Numerical modelling

The observations of the non-phasematched THG were used to test the generalized nonlinear envelope equation model of broadband ultrashort pulse propagation recently developed in [25]. Specifically, we model our experiments using the nonlinear envelope equation expressed in the laboratory

frame as:

$$\frac{\partial U}{\partial z}+\frac{\alpha}{2}U-\sum_{k\geq 0}\frac{\mathrm{i}^{k+1}}{k!}\beta_k\frac{\partial^k U}{\partial t^k}=\mathrm{i}\gamma\left(1+\mathrm{i}\tau_{\mathrm{ss}}\frac{\partial}{\partial t}\right)$$
$$\times\left((1-f_{\mathrm{R}})\left[|U|^2+\frac{1}{3}\mathrm{e}^{-\mathrm{i}2\omega_0 t}U^2\right]U+f_{\mathrm{R}}g(z,t,U)\right). \quad (1)$$

Here $U(z,t)$ is a forward propagating envelope normalized such that $|U|^2$ yields the instantaneous power in W. On the left hand side, α is the linear loss and the β_k's are the Taylor series coefficients of a broadband expansion of the fibre dispersion constant $\beta(\omega)$ over the wavelength range of interest. On the right-hand-side, the terms proportional to $|U|^2U$ and U^3 describe self-phase modulation and THG respectively. The nonlinear coefficient $\gamma=\omega_0 n_2/cA_{\mathrm{eff}}$, where the nonlinear refractive index n_2 and the effective area A_{eff} are both evaluated at the carrier frequency ω_0. The envelope self-steepening timescale τ_{ss} describes the dispersion of the nonlinear response, and $g(z,t,U)$ is a generalized Raman response function with $f_{\mathrm{R}}=0.18$ [25]. Quantum noise effects were included through a phenomenological one photon per mode background on the input pulse [10].

Comparison with the numerical solution of Maxwell's equations has shown that this propagation equation accurately models propagation effects over bandwidths many times the carrier frequency at intensities below the damage threshold of fused silica. It thus would be expected to realistically describe the simultaneous pump pulse spectral broadening and non-phasematched harmonic generation that we observe in our experiments. (Note that typical modal intensities in our experiments are around 10^{15} W m^{-2}, orders of magnitude less than the material damage threshold of fused silica around 10^{18} W m^{-2}). The fibre parameters used in the simulations were $\gamma=9.4$ W^{-1} km^{-1}, $\tau_{\mathrm{ss}}=1.67$ fs, $\alpha=0$ m^{-1} and the dispersion was determined over the extended wavelength range 300–3000 nm using beam propagation techniques based on a model refractive index profile for the fibre constrained to the manufacturer's dispersion data over 1500–1600 nm. The simulations directly included the global dispersion $\beta(\omega)$ in the numerical integration of the GNEE but Fig. 3 shows the corresponding group velocity dispersion parameter (in ps/nm km) for completeness. The input pulses used were based on FROG measurements of the experimental intensity and phase profile.

Simulations were first used to provide insight into the general dynamics of the THG generation process, and Fig. 4 shows results from the numerical solution of (1) plotting the evolution of the THG signal at 520 nm over a propagation distance of 5 mm. The pulses used in these simulations had near hyperbolic secant profiles with 90 fs FWHM and peak power of 16 kW. The observed oscillatory behaviour is typical of a non-phasematched process, and the inset shows details of the oscillations at the expected coherence length of $L_{\mathrm{coh}}=2\pi/|\Delta\beta|=2\pi/|\beta_{3\omega 0}-3\beta_{\omega 0}|\approx 15$ μm. The decrease in the oscillation contrast over a length scale of ~ 500 μm arises from the group velocity mismatch between the fundamental and harmonic fields [19, 20]. These simulations confirm that our experiments with fiber lengths greater than 600 μm are carried out in a regime where these coherence oscillations on a 15 μm length scale are not observed.

Figure 5 presents specific comparisons between simulation and experiment, plotting the experimentally-measured and simulated spectra after a propagation distance of (a) 600 μm and (b) 4.5 cm. In both cases, the simulations reproduce well both the observed supercontinuum spectral broadening of the pump pulse as well as the structure of the generated third harmonic, specifically the double-peaked THG peak was observed at 4.5 cm propagation. Additional simulations for the 600 μm case were also carried out to study the quantitative variation in the generated THG power as a function of input pulse power and the simulation results (which exhibit the expected cubic dependence on input power) are superimposed on the experimental results in Fig. 2c as the dashed line.

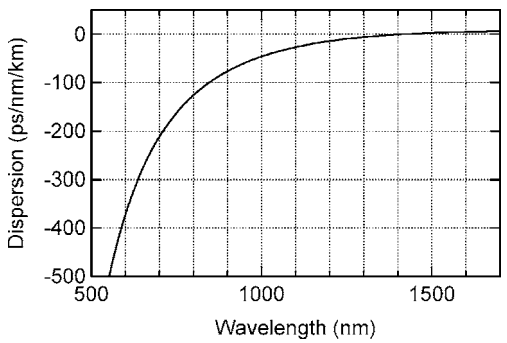

FIGURE 3 Group velocity dispersion curve used in simulations of pulse propagation in HNLF. The fibre zero dispersion wavelength is around 1410 nm and at 1560 nm the group velocity dispersion and third-order dispersion are $\beta_2=-5.4$ ps^2 km^{-1} and $\beta_3=4.2\times10^{-2}$ ps^3 km^{-1}

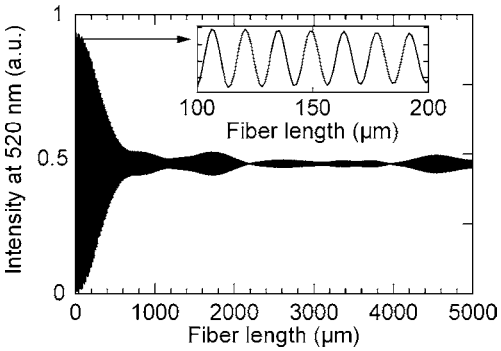

FIGURE 4 Simulation results illustrating the initial evolution of the third harmonic signal

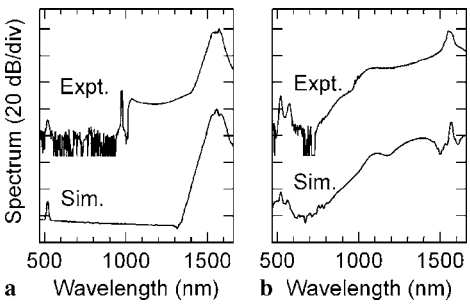

FIGURE 5 Comparison between experimental and simulated spectra as shown for spliced HNLF segment lengths of (**a**) 600 μm and (**b**) 4.5 cm

4 Conclusions

The results in Fig. 5 are the first to directly compare experimental measurements and generalized envelope equation simulations of nonlinear spectral broadening over a spectral range extending from the pump to the third harmonic. This numerical approach is extremely convenient and complements analysis or simulation based on coupled propagation equations for the pump and third harmonic fields, particularly in cases where the fields begin to spectrally overlap as in Fig. 5b. Interestingly, we note that harmonic generation effects in optical fibres has actually been known for some time [1, 27], but the absence of appropriate broadband modelling techniques have previously precluded a detailed comparison with numerical simulations. However, our results confirming that generalized nonlinear envelope simulations can accurately describe the THG generation process lead us to expect that further combined experimental and numerical studies will yield improved insight into the nonlinear interactions in this propagation regime.

REFERENCES

1 G.P. Agrawal, *Nonlinear Fiber Optics*, 4th edn. (Academic, San Diego, 2006)
2 J.C. Knight, D.V. Skryabin, Opt. Express **15**, 15 365 (2007)
3 A.A. Sukhorukov, D.N. Neshev, Y.S. Kivshar, Opt. Express **15**, 13 058 (2007)
4 J.M. Dudley, C. Finot, D.J. Richardson, G. Millot, Nature Phys. **3**, 597 (2007)
5 J.K. Ranka, R.S. Windeler, A.J. Stentz, Opt. Lett. **25**, 25 (2000)
6 A.V. Husakou, J. Herrmann, Phys. Rev. Lett. **87**, 203 901 (2001)
7 T. Udem, R. Holzwarth, T.W. Hänsch, Nature **416**, 233 (2002)
8 A.M. Zheltikov, Usp. Fiz. Nauk. **176**, 623 (2006) (in Russian) [English translation: Phys. Usp. **49**, 605 (2006)]
9 P.S.J. Russell, J. Lightwave Technol. **24**, 4729 (2006)
10 J.M. Dudley, G. Genty, S. Coen, Rev. Mod. Phys. **78**, 1135 (2006)
11 J.K. Ranka, R.S. Windeler, A.J. Stentz, Opt. Lett. **25**, 796 (2000)
12 F.G. Omenetto, A.J. Taylor, M.D. Moores, J. Arriaga, J.C. Knight, W.J. Wadsworth, P.S.J. Russell, Opt. Lett. **26**, 1158 (2001)
13 A.N. Naumov, A.B. Fedotov, A.M. Zheltikov, V.V. Yakovlev, N.B. Skibina, L.A. Mel'nikov, V.I. Beloglazov, A.V. Shcherbakov, J. Opt. Soc. Am. B **19**, 2183 (2002)
14 F. Omenetto, A. Efimov, A. Taylor, J. Knight, W. Wadsworth, P. Russell, Opt. Express **11**, 61 (2003)
15 A. Efimov, A.J. Taylor, F.G. Omenetto, J.C. Knight, W.J. Wadsworth, P.S.J. Russell, Opt. Express **11**, 910 (2003)
16 A. Efimov, A.J. Taylor, F.G. Omenetto, J.C. Knight, W.J. Wadsworth, P.S.J. Russell, Opt. Express **11**, 2567 (2003)
17 D.A. Akimov, A.A. Ivanov, A.N. Naumov, O.A. Kolevatova, M.V. Alfimov, T.A. Birks, W.J. Wadsworth, P.S.J. Russell, A.A. Podshivalov, A.M. Zheltikov, Appl. Phys. B **76**, 515 (2003)
18 A. Efimov, A.J. Taylor, Appl. Phys. B **80**, 721 (2005)
19 A.M. Zheltikov, Phys. Rev. A **72**, 043 812 (2005)
20 A. Zheltikov, J. Opt. Soc. Am. B **22**, 2263 (2005)
21 A.A. Ivanov, D. Lorenc, I. Bugar, F. Uherek, E.E. Serebryannikov, S.O. Koronov, M.V. Alfimov, D. Chorvat, A.M. Zheltikov, Phys. Rev. E **73**, 016 610 (2006)
22 E.E. Serebryannikov, A.B. Fedotov, A.M. Zheltikov, A.A. Ivanov, M.V. Alfimov, V.I. Beloglazov, N.B. Skibina, D.V. Skryabin, A.V. Yulin, J.C. Knight, J. Opt. Soc. Am. B **23**, 1975 (2006)
23 A.A. Ivanov, D.A. Sidorov-Biryukov, A.B. Fedotov, E.E. Serebryannikov, A.M. Zheltikov, J. Opt. Soc. Am. B **24**, 571 (2007)
24 V.L. Kalashnikov, E. Sorokin, I.T. Sorokina, Opt. Express **15**, 11 301 (2007)
25 G. Genty, P. Kinsler, B. Kibler, J.M. Dudley, Opt. Express **15**, 5382 (2007)
26 B. Kibler, R. Fischer, P.A. Lacourt, F. Courvoisier, R. Ferrière, L. Larger, D.N. Neshev, J.M. Dudley, Electron. Lett. **43**, 915 (2007)
27 J.M. Gabriagues, Opt. Lett. **8**, 183 (1983)